numerically modeled as a combination of multiple Bragg peak signals and linear decomposition can disentangle different WET contributions, thus building up WET histogram at each raster point.
The Gaussian model of the lateral pencil beam profile is calculated for each raster point as convolution between beam spot and MCS models, thus defining a neighborhood on the radiography space. The MCS model is based on WET with maximum probability, typically considered in integration-mode. The integral of the WET histogram is normalized to unity, thus expressing WET probability. The WET probability, originally assigned to the raster point, is spatially distributed based on corresponding WET probabilities of adjacent raster points, weighted according to the Gaussian model of beam intensity.
Quantification is performed in comparison with list-mode in radiography space, prior to image reconstruction. Analytical and Monte Carlo simulations of proton radiographies for phantom and Computed Tomography (CT) patient data are considered.
Results: The enhancement of spatial resolution from IE-mode with respect to list-mode is observable in Fig.1. The method does not modify the typical integration-mode radiography based on WET with maximum probability for each raster point, unless at the edges where the neighborhood is not centered at the raster point position (Fig.1). On analytical simulations, WET root mean square difference of IE-mode with respect to list-mode is 9.39±0.83 mm. On Monte Carlo simulations of patient data this difference is reduced down to 3 mm because of absence of sharp anatomical details in CT data.
Conclusions: The redundancy of information collected by integration-mode detector offers possibilities to enhance spatial resolution. Similar to list-mode radiographies, the spatial resolution will be optimized by tomographic image reconstruction algorithms embedding this spatial information. Quantification will be performed in both radiography end tomography spaces, with respect to MCS-free gold standard.
Keywords: Proton radiography and tomography, integration-mode and list-mode configurations, spatial resolution

Acknowledgments
BMBF (01IB13001, SPARTA); DFG (MAP); DFG (VO 1823/2-1)

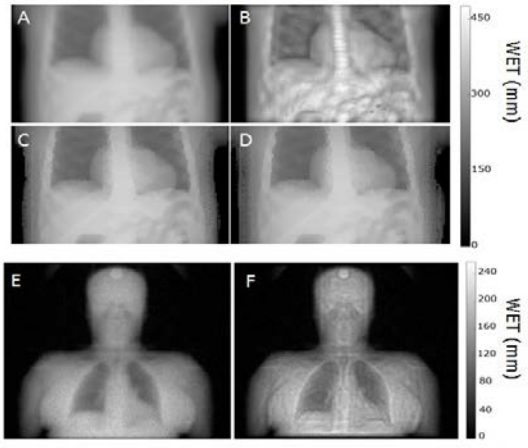

Fig.1. Analytical simulation in phantom: list-mode radiography (A), integration-mode radiography corresponding to the maximum WET probabilities (C), enhanced integration-mode radiography (B) and its maximum WET probabilities (D). Monte Carlo simulation in patient data: list-mode radiography (E) and enhanced integration-mode radiography (F).

97

Hybrid TOF-PET/MRI local transceiver coil

B. Głowacz[1,@], M. Zieliński[1] D. Alfs[1], T. Bednarski[1], P. Białas[1], E. Czerwiński[1], A. Gajos[1], M. Gorgol[2], B. Jasińska[2], D. Kamińska[1], Ł. Kapłon[1,3], G. Korcyl[1], P. Kowalski[4], T. Kozik[1],W. Krzemień[5] , E. Kubicz[1], M. Mohammed[1], M. Pawlik-Niedźwiecka[1] , S. Niedźwiecki[1], M. Pałka[1], L. Raczyński[4], Z. Rudy[1], O. Rundel[1], N. G. Sharma[1], M. Silarski[1], A. Słomski[1], A. Strzelecki[1], A. Wieczorek[1,3], W. Wiślicki[4], B. Zgardzińska[2], P. Moskal[1]
[1]Faculty of Physics, Astronomy and Applied Computer Science, Jagiellonian University, S. Łojasiewicza 11, 30-348 Kraków, Poland,
[2]Department of Nuclear Methods, Institute of Physics, Maria Curie Sklodowska University, Pl. M. Curie-Sklodowskiej 1, 20-031 Lublin, Poland
[3]Institute of Metallurgy and Materials Science of Polish Academy of Sciences, W. Reymonta 25, 30-059 Kraków, Poland
[4]Świerk Computing Centre, National Centre for Nuclear Research, A. Soltana 7, 05-400 Otwock-Świerk, Poland
[5]High Energy Physics Division, National Centre for Nuclear Research, A. Soltana 7, 05-400 Otwock-Świerk, Poland
[@] - bartosz.glowacz@cern.ch

Purpose: Nowadays devices based on the detection of nuclear and electromagnetic radiation are in common use for the diagnosis of the interior of the human body. The most technologically advanced are positron emission tomography (PET), computed tomography (CT) and magnetic resonance imaging (MRI). In order to enhance diagnostic capabilities PET and MRI devices were combined into a single hybrid device providing an access to both metabolic and morphological information during a single examination. Typically the PET detectors are placed inside the diagnostic tunnel of the MR scanner. In spite of a possibility of the whole body and simultaneous PET and MR imaging the problem of the local MR transmit-receiver (transceiver) coils use still remains. Such coils are designed to be close to the imaged object, thus enhancing the MR image quality in comparison to the whole body coil use that is built in the MR scanner.
The coils are made of plastic parts and metal conductors which are on the way of gamma quanta flying from the annihilation point in the patients body to the scintillating material. This fact could cause the worsening of a spatial resolution of the PET diagnostic images, as the field-of-view (FOV) for the PET detectors is limited and gamma quanta scattering increases.
Material and methods: Therefore, it would be favorable to construct a single device consisting of a wire transmit-receive MR antenna integrated with the PET detectors that are able to register gamma quanta simultaneously with the magnetic resonance scan without mutual disturbance between the two detection systems and limiting the loses of images quality met so far.
We propose a solution based on a strip TOF-PET tomograph concept [1] comprising multiple PET detection modules, built from polymer scintillation strip ended with silicon photodetectors, arranged circumferentially inside the working volume of the MRI local transceiver coil. The adaptive of the polymer scintillators in both shape and size properties allows for a use of a standard MRI coils constructions to be combined with PET detection system with only a minor changes in the overall MRI coil dimensions, that do not influence the coil shape, geometry and material properties optimized so far.
The detection electronics based on silicon photodetectors and digital signal processing system [2] will operate in high static magnetic fields as well as radiofrequency waves environment of MR scanner, for instance. Such hybrid coil could be used in existing MRI systems extending its functionality by the PET imaging feature.
Conclusions: In the presentation the problem of local MR coils use in PET detectors will be introduced referring to the technology developed so far, underlying its weaknesses and limitations. Starting with the strip TOF-PET concept the idea of hybrid PET/MR local coil construction will be presented in details emphasizing the advantages over the former solutions [3].

Keywords: PET-MR, hybrid PET-MR coil, strip-PET

References:

[1] "STRIP-PET: Concept of TOF-PET scanner based on polymer scintillator strips", P.Moskal et al. Nuclear Medicine Review 15 (2012) A61-A63
[2] "A novel method based solely on FPGA units enabling measurement of time and charge of analog signals in Positron Emission Tomography". M.Pałka el al. Bio-Alg. and Med-Systems Vol. 10, 1,(2014) 41-45
[3] "Hybrid TOF-PET/MRI transceiver coil", B.Glowacz, M.Zielinski, P.Moskal, Patent application PZ/3256/RW/PCT (2015)

98

Treatment outcome in patients treated with single-dose irradiation (SDRT) for oligometastatic disease

Carlo Greco [1]
[1] Department of Radiation Oncology, Chamapalimaud Centre for the Unknown, Lisbon

Purpose: to analyze treatment outcome following Single-Dose Image-Guided Radiotherapy (SDRT) using PERCIST criteria based on 18-F-fluoro-2-deoxy-D-glucose PET Standardized Uptake Value (SUV_{max}) assessments in patients with limited extra-cranial metastatic disease.
Methods and Materials: 259 lesions in 101 consecutive patients with early metastatic disease with less than five lesions at initial presentation (mean 2.1, range 1-5 lesions) were treated between November 2011 and March 2015 with SDRT. Mean and median PTV volume were 40.6 and 18.1 cm^3 (range, 1.3-339), respectively. PTV prescription dose was 24Gy. Of the 101 patients, 56 (55%) of had a solitary metastasis at the time of first treatment. While the majority of the patients received only one treatment, 27% (27/101) received additional treatments (mean 1.4, median 1 range, 1-7) for relapses elsewhere. Thus, the mean number of lesions for the entire population was 2.6 (range, 1-13). SUV_{max} were acquired at the time of FDG-PET/CT planning before SDRT, at 3 and 6 months post-treatment and every 6 months thereafter. Treatment outcome was assessed by PERCIST criteria, with metabolic relapse defined as any increase of SUV_{max} >20% above nadir level. All metabolic relapses were confirmed by morphologic imaging. Lesions had a minimum of 2 post-treatment scans (mean 4; range 2-11) with a minimum follow-up of 6 months.
Results: actuarial 2- and 3-year overall survival for this cohort were 71% and 64%, respectively. At a median follow-up of 16.1 months (range, 6.7- 43.5 months), 6% (15/259) of lesions developed PERCIST failure within the irradiated region yielding a 3-year actuarial freedom of local relapse of 90%. Mean time to local relapse was 9 months. All recurrences occurred within the first 19 months. The mean percentage increase in SUV_{max} in relapsing lesions was 429% (range, 28% - 2530%). The mean and median baseline SUV_{max} were 8.9 and 6.9, respectively (range, 0.7-52.0). At 3 months post-SDRT, 15% (40/259) of the lesions had a >90% reduction in SUVmax (PERCIST complete metabolic response). SUV_{max} declines >75% ($\Delta SUV_{max\ >75\%}$) was significantly associated with freedom from metabolic relapse at 3 years ($p = 0.02$). Lesions with with $\Delta SUV_{max\ >75\%}$ had 94% local control at 36 months *vs*. 77% for $\Delta SUV_{max\ \leq 75\%}$. On univariate analysis, no correlation was found with primary tumor histology, metastasis site, PTV volume or ongoing systemic treatment and the likelihood of local relapse free survival.
Conclusion: These results confirm that high dose SDRT provides long-term local relapse-free survival using objective PERCIST therapeutic response criteria in patients with early metastatic disease. Additionally, they provide preliminary evidence that an early evaluation in metabolic changes post-SDRT may serve as a useful prognostic tool in the assessment of lesions treated with ablative intent.

99

How to produce scandium-44 efficiently?

C. Duchemin[1], A. Guertin[1], F. Haddad[1,2], N. Michel[1,2], V. Metivier[1]
[1] Laboratoire SUBATECH, Ecoles des Mines de Nantes, Université de Nantes, CNRS/IN2P3, 4 rue Alfred Kastler, 44307 Nantes cedex 3 - FRANCE
[2] GIP ARRONAX, 1 rue Aronnax, 44817 Saint-Herblain cedex – FRANCE

Purpose: Among the large number of radionuclides of medical interest, Sc-44 is promising for PET imaging. Either the Sc-44g or the Sc-44m can be used for such applications, depending on the molecule used as vector. This study compares the production rates of both Sc-44 states, when protons or deuterons are used as projectiles on an enriched calcium-44 target for 3 scenarios: the production of Sc-44g for conventional PET imaging, its production for the new 3 γ imaging technique developed at the SUBATECH laboratory and the production of Sc-44m to be used as Sc-44m/Sc-44g in vivo generator for antibody labelling.
Materials/methods: Experimental production cross section have been measured up to 34 MeV for the Ca-44(d,2n)Sc-44m,Sc-44g reactions, using the stacked-foil technique [1] and gamma-spectrometry, at the ARRONAX cyclotron [2]. The stacks were made of $Ca\text{-}44CO_3$ as targets and aluminum foils as degraders. Monitor foils were made of natural titanium in order to use the IAEA recommended cross section of the Ti-nat(d,x)V-48 reaction. Some results on the production of K-42,43 and Sc-43 have also been obtained but not in all the targets as the main objective was first to properly measure the activity of Sc-44m and Sc-44g. The results are compared with the TALYS code [3] version 1.6. Based on these experimental data, the Thick-Target production Yields (TTY) of Sc-44m and Sc-44g are calculated and compared with those for the proton route for the 3 scenarios [4].
Results: Experimental cross section values have been obtained for the first time for Ca-44(d,2n)Sc-44m,Sc-44g reactions with some information on Sc-43 and K-42,43 also produced during the irradiation. The TALYS results are close to the experimental values for the Ca-44(p,n) and Ca-44(d,2n) reactions whereas it is not able to reproduce the data for the production of potassium isotopes. Our new experimental results have shown that the Sc-44m/Sc-44g cross section and TTY ratios are higher with deuterons than with protons, whatever the incident beam energy.
Conclusions: This study shows that the use of a proton beam is the best choice, as compared to deuterons, to produce Sc-44g for PET imaging using peptides or small molecules with rapid distribution in the body. For the 3 γ imaging technique, Sc-44g has to be produced with protons of 15 MeV to limit the background generated by Sc-44m and Sc-43 decay. The production of the Sc-44m to be used as Sc-44m/Sc-44g in vivo generator for antibody labelling required the highest Sc-44m production rate, with a limited amount of Sc-44g directly produced. The production of Sc-44m is advantageous with deuterons as projectiles, using a calcium-44 carbonate target. Sc-44m can be produced with a 15 MeV deuteron. A higher amount of Sc-44m is produced with a 30 MeV deuteron beam and some cooling time, before the extraction and separation processes, allows to significantly reduce the contribution of directly produced Sc-44g and Sc-43.

Keywords: Sc-44g for PET, 3γ imaging, Sc-44m/Sc-44g in vivo generator

References:
[1] Duchemin C, Guertin A, Haddad F, Michel N and Métivier V. Cross section measurements of deuteron induced nuclear reactions on natural tungsten up to 34 MeV. Appl. Radiat. Isot. 97 52–8, 2015
[2] Haddad F., Ferrer L., Guertin A., Carlier T., Michel N., Barbet J., and Chatal J.F. Arronax a high-energy and high-intensity cyclotron for nuclear medicine. Eur. J. Nucl. Med. Mol. Imaging, 35:1377–1387, 2008
[3] Koning A.J. and Rochman D. Modern nuclear data evaluation with the TALYS code system. Nucl. Data Sheets, 113, 2012
[4] Duchemin C, Guertin A, Haddad F, Michel N and Métivier V. Production of scandium-44m and scandium-44g with deuterons on calcium-44: cross section measurements and production yield calculations. Phys. Med. Biol. 60 (2015) 6847–6864, 2015